Multiphysics Design of Triple 3-Phase PMSM for Ultra-High Speed Elevator Applications

Jae-Han Sim, Dong-Gyun Ahn, Dae-Kee Kim, Dong-Kyun Son, Saekyeol Kim, Jung-Pyo Hong, *Senior Member*, *IEEE*, and Tae Hee Lee

***Abstract* – This paper proposes triple three-phase surface-mounted permanent magnet synchronous machine (PMSM) as a fascinating solution for ultra-high speed (1260m/min) elevator direct-drive applications and describes its multiphysics design p-rocedure. Particularly, the design procedure focused not only on achieving the required output power, but also on decreasing the low frequency radial vibration and the torque pulsation to ame-liorate the riding comfort of occupants. As a result, the 144-slot and 40-pole combination with 20 electrical degree of phase shift was chosen considering the following criteria: winding factor, frequency and space order of radial force, cogging torque, and optimal phase shift between adjacent sets. In addition, the rotor diameter was rearranged to enhance power factor and efficiency. The robust design optimization was also carried out to ensure the manufacturing uncertainties. As a result, an optimum model was obtained and analyzed through FEA in order to justify the aforementioned design procedure. Finally, it was compared with the 144-slot and 32-pole prototype to validate its effectiveness.**

***Index Terms*—efficiency, power factor, riding quality, robust design optimization, surface-mounted PMSM, torque pulsation, triple three-phase, ultra-high speed elevator, vibration.**

I. INTRODUCTION

THE NdFeB-based permanent magnet synchronous machine (PMSM) is attractive alternative to the ferrite- or the SmCo-based machines [1]-[3]. As compared with such PMs, the NdFeB features the superior residual induction and the coercive force. Also, it has a strength in the temperature properties thanks to its superior thermal coefficients [2], [4]. As a result, the NdFeB-based surface-mounted PMSM has usually been used in ultra-high speed elevator direct drive applications because it shows the higher power density and the lower vibration than the other electrical machines [5], [6].

Fig. 1 shows the common structure of the ultra-high speed elevator direct drive system where an independent machine room equipped with the intermediate gears does not exist. The triple three-phase traction machine is linked to electronic control system in Fig. 2 and delivers its output power directly to the drive sheave, which a pulley with grooved wheel for holding up the high-tensile-steel hoisting ropes. The hoisting ropes lift up or down an elevator car and a counter-weight. Here, the traction machine play an essential role in operating the elevator car because there are no any supports from the intermediate power transmission gears. Consequently, the electromagnetic and vibratory characteristics of the traction machine have a significant effect on the riding quality and should be reflected together in the design process.

The authors are with the Department of Automotive Engineering, Hanyang University, Seoul, South Korea (e-mail: ental@hanyang.ac.kr; ahllen@hanyang.ac.kr; haunters@hanyang.ac.kr; thsehdrbs92@gmail.com; kyeol8805@gmail.com; hongjp@hanyang.ac.kr; thlee@hanyang.ac.kr)

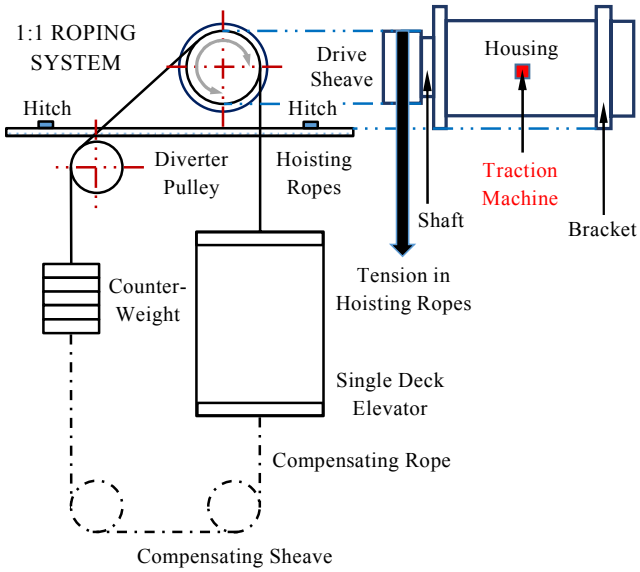

Fig. 1. Schematic view of ultra-high speed elevator direct drive system.

Not many academic papers have discussed the design pr-ocess of the traction machine for the ultra-high speed elevator direct drive application considering both its electromagnetic and vibratory properties. A conventional DC current driven machine was presented in [7]. In contrast, it usually generates higher torque ripple and higher radial vibration that make the passengers feel uncomfortable than the AC current driven m-achines. Wang *et al.* [8], [9] and Jung *et al.* [10] only dealt with the electronic control method of the surface-mounted PMSM. As another substitute, the academic authors of [11]-[16] discussed various types of the linear machines for the ropeless elevators. The installation expenses of such machine, however, are much more expensive than those of the rotating machines and they are not lucrative.

This paper deals with the multiphysics design procedure of triple three-phase surface-mounted PMSM for ultra-high speed elevator applications. The design procedure considers both the electromagnetic and vibratory characteristics which influence the performance and the riding quality. The electro-magnetic characteristics are related to electromagnetic torque, output power, power factor, and efficiency. The vibratory pr-operties are related to torque ripple and radial vibration. Also, the robust design optimization was also carried out to guaran-tee the manufacturing uncertainties. As a result, the 144-slot and 40-pole combination with 20 electrical degree of phase shift was chosen considering the following criteria: winding factor, frequency and vibration order of radial force, cogging torque, and optimal phase shift between adjacent set. It was compared with 144-slot and 32-pole prototype.

978-1-5386-2477-7/18/$31.00 ©2018 IEEE

II. System Description and Design Requirements

Fig. 2 describes the electronic control system of the triple three-phase traction machine. It consists of three individual PWM inverters and current controllers where i^*_{a1} denotes the command value and i_{a1} the input value. As shown in Fig. 2, they can operate independently regardless of adjacent sets.

Table I shows a summarization of the design requirements of the traction motor developed for the 30-passenger gearless elevator applications. The payload or the passenger capacity is 2 ton and the total mass of an entire system is assumed to be 5 ton including that of the hoisting ropes, the elevator car, the counter-weight part, and the miscellaneous devices. The minimum diameter of the shaft is restricted to 1000 mm since the shaft linked to the drive sheave should sustain the total mass. Otherwise, there exists the static eccentricity of the shaft that results in the air-gap irregular length, the unbalanced electromagnetic force, and then the high radial vibration.

Moreover, the vertical speed of the elevator car is defined as the product of the rotating speed of the traction motor and the outer circumference of drive sheave. This work focuses on a gearless elevator with an ultra-high speed (1260 m/min) for the skyscrapers. There are three types of drive modes in a time-speed domain over a period of operating time as shown in Fig. 3: acceleration, constant or rated speed, and deceleration regions. The acceleration and the deceleration speeds are limited not to make the passengers feel uncomfortable.

III. Slot and Pole Combination

A. Prerequiste Condition (Optimal Phase Shift)

The operating frequency f of the electronic drive system should be proportional to the rotating speed (rev/min) and the rotor pole number of the traction machine. An increasingly rising operating frequency especially makes the electric drive system burdensome in controlling the rotating speed [17]. In addition, its switching frequency $f_{switching}$ (6 kHz) has to be 50 times over than the operating frequency. It means that at least 50 times of switching is required for producing a sinusoidal output voltage waveform at the desired frequency in PWM control [17]. The maximum number of magnetic poles, p_{max}, is eventually limited by the maximum rotating speed of the traction motor, n_{max}, and the capability of the electric control system as described in (1).

TABLE I
Design Requirements for Rated and Maximum Load Conditions

Division	Rated Condition	Maximum Condition	Unit
Passenger / Payload	30 / 2000		kg
Rated car speed	1260		m/min
(PMSM speed)	291		rev/min
Outer stator diameter	1340		mm
Stack length	300		mm
Average torque	8500	42500	Nm
Output power	259	1295	kW
Phase current	200	1000	A_{rms}
Line-to-line voltage	450	450	V_{rms}
Power factor	≥ 95	≥ 65	%
Efficiency	≥ 95	≥ 95	%

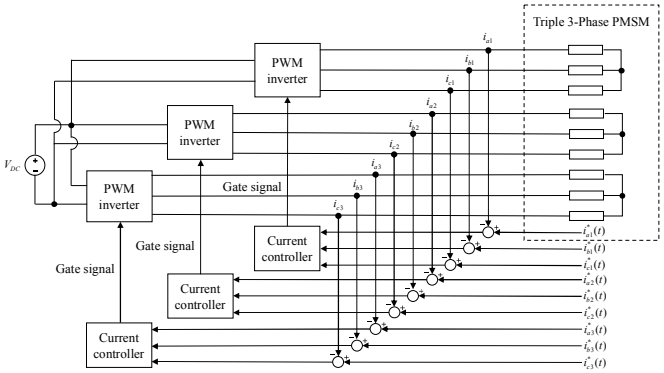

Fig. 2. Electronic control system of triple three-phase traction machine for ultra-high speed elevator drive system.

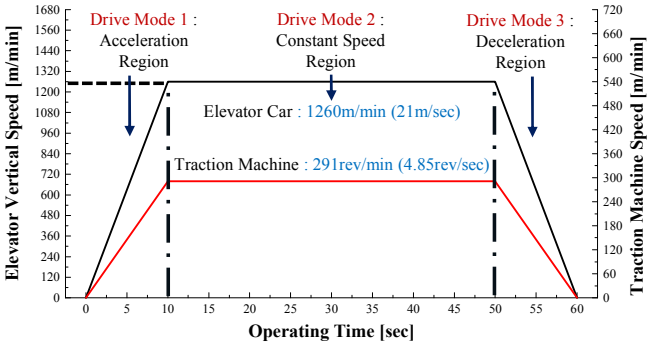

Fig. 3. Driving pattern of the ultra-high speed (1260m/min) elevator and its traction machine (291rev/min).

$$p_{max} = (120 \cdot f) / n_{max} \qquad \left(f_{switching} > 50 \cdot f\right) \tag{1}$$

Based on the controllability and the geometric constraints, several slot and pole combinations with less than 48 magnetic poles were examined in this paper. It is assumed that each set windings are wye-connected to eliminate the 3rd, 6th, 9th, and etc. harmonic components of the line-to-line back electromotive force (BEMF) and double-layered to produce the more sinusoidal magneto-motive force. Fig. 4 illustrates the general layout of N phase and k multiple windings. In the case of triple three-phase winding, the phase shift between the adjacent sets is restricted to 20 or 40 electrical degree so as to minimize the torque harmonics [18].

B. Winding Factor

The slot and pole combination has a significant effect on the winding layout from which the fundamental component k_{w1} and the harmonic components k_{wn} (n: natural number, ≠1) of the winding factor can be calculated. They are simply defined as the product of the distribution factor k_{dn}, the pitch factor k_{pn}, the skew factor k_{sn} as in (2) [19], [20].

$$k_{wn} = k_{dn} \cdot k_{pn} \cdot k_{sn} \tag{2}$$

Particularly, the 1st component defines the effective turns of the phase windings and contributes to generate the line-to-line BEMF and the electromagnetic torque. To maximize the torque and power density, only the combinations with more than 0.9 of the 1st component were covered in this work.

The 18th, 36th, and other harmonics of the electromagnetic torque are typically generated in the 9-phase AC machines.

Such harmonics directly affect the oscillation of the elevator car and make the passengers uncomfortable. Moreover, it was understood that the 18th harmonic was the most dominant out of the torque harmonics. It is mainly induced by the 17th and 19th harmonics of the line-to-line BEMF. Those components can be reduced by selecting the slot and pole combinations having the low values of the 17th and 19th harmonics of the winding factor. The stator one slot skew is applied to all the combinations to reduce the high harmonics effectively.

C. *Frequencies and Space Orders of Radial Force*

The vibration generated from the traction machine of the elevator make passengers inconvenient. Thus, to make the elevator system stable, it is important to minimize it. In this section, the slot and pole combination to minimize vibration will be determined by calculating vibration orders.

The radial electromagnetic force based on Maxwell Stress Tensor is the main cause of motor vibration and its frequency is $2f$ where f is the operating frequency. The vibration order indicates the spatial distribution of the radial electromagnetic force around the entire air gap area. The following equation (3) indicates the relationship between the deformation of the stator core Δd and the vibration order r [21].

$$\Delta d \propto \frac{1}{r^4} \tag{3}$$

That is, to minimize vibration, the lowest vibration order should be maximized. The vibration order can be determined by considering the main causes of the radial electromagnetic forces as following four sources.

i) r_1 excited by the stator ν and rotor μ harmonics
ii) r_2 excited by the rotor μ harmonics in slotted structure
iii) r_3 excited by the rotor harmonics of the same number μ
iv) r_4 excited by the stator harmonic of the same number ν

The vibration orders from r_1 to r_4 can be calculated using (4)-(6) according to the slot and pole combination.

$$r_1 = \frac{P}{2}\cdot(\nu \pm \mu),\quad \mu = 2\cdot\frac{|0.5\cdot r_2 \pm N_s|}{P},\quad r_3 = P\cdot\mu,\quad r_4 = P\cdot\nu \tag{4}$$

where $$\nu = 1 \pm k\frac{2N_s}{P} \quad (k = 0, 1, 2, 3, \cdots) \tag{5}$$

$$\mu = 2k \pm 1 \quad (\text{for } 2f) \tag{6}$$

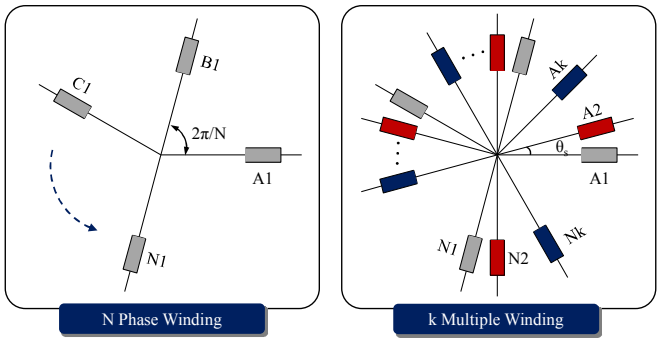

Fig. 4. General layout of N phase and k multiple windings.

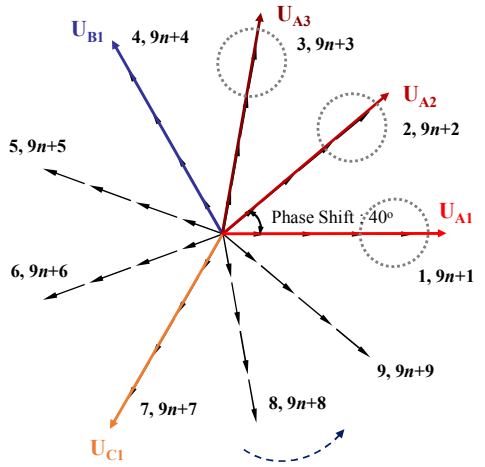

Fig. 5. Voltage vector diagram of 144-slot and 32-pole combination. It has 40 electrical degree of phase shift between the adjacent sets.

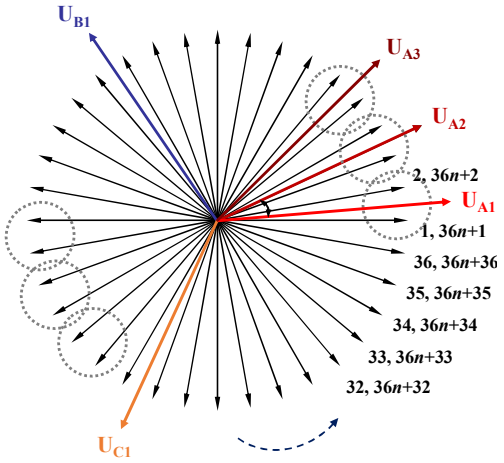

Fig. 6. Voltage vector diagram of 144-slot and 40-pole combination. It has 20 electrical degree of phase shift between the adjacent sets.

In conclusion, comparing lowest vibration and magnitude of radial magnetic force, the 144-slot and 40-pole machine where the phase shift is 20 degree as shown in Fig. 6 exhibits the lowest deformation compared to other combinations including the 144-slot and 32-pole prototype shown in Fig. 5.

D. *Cogging Torque*

The cogging torque of PMSM is a reluctance torque due to the interaction between the rotor PMs and the stator slots as the PMs rotate past the slot openings. It is also called as the zero-current torque or the detent torque. Its effect can be decreased by the motor moment of inertia at high speed regions. In contrast, the cogging torque is especially dominant at low speed regions at which the traction machine for gearless elevators drives. It is a source of producing the torque ripple.

Such cogging torque shows the following two features: i) Its periodicity per revolution is proportional to least common multiple of the number of magnetic poles and the number of the stator teeth; ii) Its amplitude is inversely proportional to that component. In other words, the higher the least common multiple is, the smaller the amplitude of the cogging torque is. It could be considered as one of the design factors in order to decrease the torque ripple in determining the slot and pole combination to be covered. Consequently, 144-slot and 40-pole combination was chosen considering the criteria above.

IV. Power Factor and Efficiency

In nonsalient-pole machines, e.g. surface-mounted PMSM, there is slight difference between the *d*irect- and *q*uadrature-axis inductances. Such machines only produce the magnetic torque and do not need the *d*-axis current control if a field-weakening control is not required. In this case ($i_d = 0$), the *d*- and *q*-axis voltage equations are shown in (7) and (8), respectively, based on the equivalent circuit method [2], [17].

$$\begin{bmatrix} v_d \\ v_q \end{bmatrix} = R_a \begin{bmatrix} 0 \\ i_{oq} \end{bmatrix} + \left(1 + \frac{R_a}{R_c}\right) \begin{bmatrix} v_{od} \\ v_{oq} \end{bmatrix} + p \begin{bmatrix} L_d & 0 \\ 0 & L_q \end{bmatrix} \begin{bmatrix} 0 \\ i_{oq} \end{bmatrix} \tag{7}$$

$$\begin{bmatrix} v_{od} \\ v_{oq} \end{bmatrix} = \begin{bmatrix} 0 & -\omega L_q \\ \omega L_d & 0 \end{bmatrix} \begin{bmatrix} 0 \\ i_{oq} \end{bmatrix} + \begin{bmatrix} 0 \\ \sqrt{3/2}\,\omega\psi_f \end{bmatrix} \tag{8}$$

where $$i_{oq} = i_q - i_{cq}, \qquad i_{cq} = \frac{\omega \cdot \left(\sqrt{3/2}\,\psi_f + L_d i_{od}\right)}{R_c} \tag{9}$$

$$i_a = i_q \le I_{am}, \qquad v_a = \sqrt{{v_d}^2 + {v_q}^2} \le V_{am} \tag{10}$$

In the preceding equations, v_d and v_q are the *d*- and *q*-axis voltages, v_{od} and v_{oq} are the *d*- and *q*-axis induced voltages, L_d and L_q are the *d*- and *q*-axis inductances, i_{cq} and i_{oq} are the *q*-axis core loss and magnetizing currents, p is the differential operator as d/dt, R_a is the phase resistance of the armature winding, R_c is the equivalent core loss resistance, ω is the electrical frequency, ψ_f is the maximum flux linkage of the PM, and V_{am} and I_{am} are the maximum terminal voltage and input current. The magnetic torque T can be expressed as in (11). The finite element analysis (FEA) was used to calculate L_d, L_q, R_c, and ψ_f, according to the input current.

$$T = \frac{P}{2} \cdot \left(\vec{\psi}_o \times \vec{i}_o\right) = \frac{P}{2} \cdot \begin{vmatrix} \vec{a}_x & \vec{a}_y & \vec{a}_z \\ \sqrt{3/2}\,\psi_f & L_q i_{oq} & 0 \\ 0 & i_{oq} & 0 \end{vmatrix} = \frac{P}{2}\sqrt{3/2}\,\psi_f i_{oq} \tag{11}$$

It can be assumed that the term R_a/R_c in the voltage equation (7) is almost zero because R_c is much more higher than R_a. Its high equivalent resistance is based on low core loss at low speeds. Then, the power factor PF and the efficiency η can be indicated as in (12) and (13), respectively.

$$PF = \frac{v_q}{\sqrt{{v_d}^2 + {v_q}^2}} = \frac{R_a i_{oq} + \sqrt{3/2}\,\omega\psi_f}{\sqrt{\left(-\omega L_q i_{oq}\right)^2 + \left(R_a i_{oq} + \sqrt{3/2}\,\omega\psi_f\right)^2}} \tag{12}$$

$$\eta = \frac{W_{out}}{W_{in}} \cdot 100\% = \frac{W_{out}}{W_{out} + W_{copper} + W_{iron} + W_{mech}} \cdot 100\% \tag{13}$$

Once the number of magnetic poles and the rotating speed of traction motor were determined, the electrical frequency ω has an unchanged value. The *q*-axis inductance L_q, representing v_d, is proportional to the square of series turns per phase. The armature winding resistance R_a and the maximum flux linkage by the PM, representing ψ_f, are proportional to series turns per phase. Here, the magnetic flux, not flux linkage, by the PM is consistent. Eventually, the series turns per phase should be minimized to maximize the power factor in (12). Likewise, the copper loss is minimized and the efficiency is maximized if the series turns per phase is minimized.

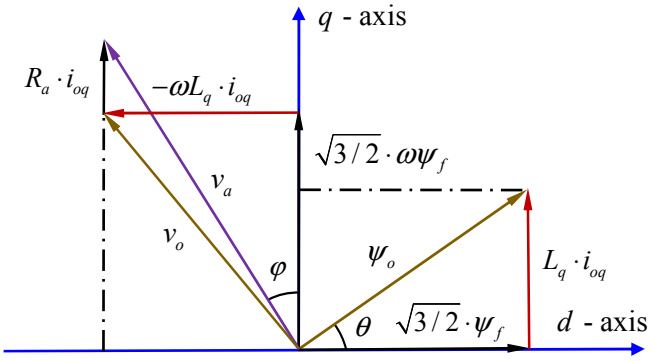

Fig. 7. Vector diagram of surface-mounted PMSM.

In electric power systems, a load with a low power factor draws more current than a load with a high power factor for the same amount of useful power transferred. Therefore, the power factor and efficiency were considered as the crieteria. Fig. 7 describes the corresponding vector diagram.

V. Robust Design Optimization (RDO)

Robust design techniques have been developed to improve product quality while maximizing its performance and satisfying other design constraints. Robust design is a design that is insensitive to variations of design variables and design parameters. There are two popular methodologies applied to electrical machines. The first is the Taguchi method, which employs orthogonal array technique to evaluate candidate design based on signal-to-noise ratio. Signal-to-noise ratio is a metric which is used to select the best design among the potential designs. Even though Taguchi method can be easily applied, there are two main limitations. The continuous design space of the problem is not considered and only the discrete design space in design of experiments (DOE) is used to find the robust design. The constraints are not formulated in this method. Because of these disadvantages, the RDO is widely employed for electrical machines [22]. This method provides the robust optimum point in the continuous design domain while satisfying all the design constraints. The general formulation of RDO can be written as (14)-(16).

$$\min_{x \in R^n} F\left(\mu_f(\mathbf{x},\mathbf{p}), \sigma_f(\mathbf{x},\mathbf{p})\right) \tag{14}$$

subject to $$g_j(\mathbf{x},\mathbf{p}) \le g_j^t, \quad j = 1,\cdots,m \tag{15}$$

$$x_i^L \le x_i \le x_i^U, \quad i = 1,\cdots,n \tag{16}$$

where $\mathbf{x}$ is the design variable vector, $\mathbf{p}$ is design parameter vector, μ_f and σ_f are the mean and standard deviation of the objective function. g_j and g^t_j are the constraint function and its target value while m and n are the number of constraints and design variables. In robust design optimization, a new function that consists of the mean and standard deviation of the objective function should be defined. In this paper, the weighted sum method, which is popular due to simple and easy formulation [23]. The function F is defined as in (17).

TABLE II
DEFINITION OF DESIGN VARIABLES AND UNCERTAINTIES

No.	Name	Lower bound	Upper bound	Uncertainty σ	Unit
1	Pole Arc	7	8	-	
2	Eccentric radius	0	450	-	mm
3	PM thickness	8	9.5	0.1	mm
-	Air gap	3.5		0.033	mm

$$F = w_1\mu_f(\mathbf{x},\mathbf{p})/\mu_j^* + w_2\sigma_f(\mathbf{x},\mathbf{p})/\sigma_j^* \quad (17)$$

where μ_f^* and σ_f^* are base values for the mean μ_f and standard deviation σ_f of the objective function respectively. They are used for normalization and usually have the starting values of the optimization process. w_1 and w_2 are weight factors for the mean μ_f and standard deviation σ_f of the objective function, respectively.

A. Manufacturing uncertainties

The variations of design variables or design parameters are caused by many avoidable manufacturing uncertainties in the practical production process of electrical machine. These manufacturing uncertainties result in the large variations of performances such as cogging torque and back EMF. Thus, these manufacturing uncertainties must be considered in the optimization process to improve the quality of the electrical machine. In order to perform the RDO, the manufacturing uncertainties should be identified and quantified. The normal distribution is used for manufacturing uncertainty while its standard deviation is estimated from manufacturing tolerance.

In this paper, the uncertainties of PM thickness and air gap are considered since they have a significant impact on the variations of the torque ripple. The identification and the quantification of these uncertainties have been discussed and determined by many engineers involved in the production process. As a result, the types of both probability distributions are assumed as normal distribution and their standard deviations are calculated by dividing the tolerance by 3. These are reasonable if 99.7 percent of the measurements generally fall within the tolerance limit in the manufacturing process.

B. RDO of synchronous machine

A variety of researches have been performed to study the factors which influence on the torque ripple or efficiency for synchronous machine. In this paper, 3 design variables and 1 design parameter in are considered as in Table II and Fig. 8.

The calculation of the mean and standard deviation of the objective function requires the first derivative of the objective function. It means that the second-order derivatives of the objective functions are needed in robust optimization process. Since the calculation of the second-order derivatives are computationally expensive, surrogate model technique is used. In this paper, the second-order response surface model including both interactions and squared terms are constructed using 25 design points selected by central composite design.

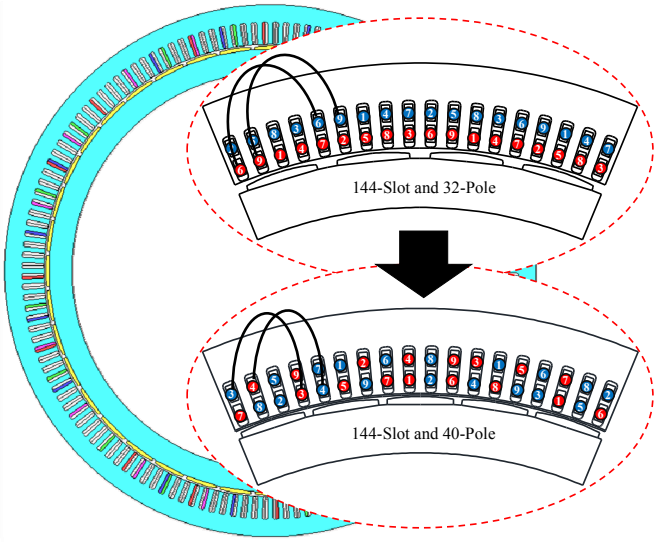

Fig. 9. Optimum model and winding layout of 144-slot and 40-pole surface-mounted PMSM. It is compared with 144-slot and 32-pole prototype.

VI. VERIFICATION

Fig. 9 describes the prototype model with 144-slot and 32-pole combination and the designed optimum model with 144-slot and 40-pole. Its finite element analysis (FEA) validation was conducted to justify the validity of the aforementioned d-esign procedure and the effectiveness of the designed model. Fig. 10 compares the line-to-line BEMF, the average torque waveforms, and their harmonics. It is shown that the designed model has their lower harmonics than the prototype under the rated and maximum load conditions. It is since the designed model exhibits the lower harmonic winding factors than the prototype. Moreover, the model has lower standard deviation

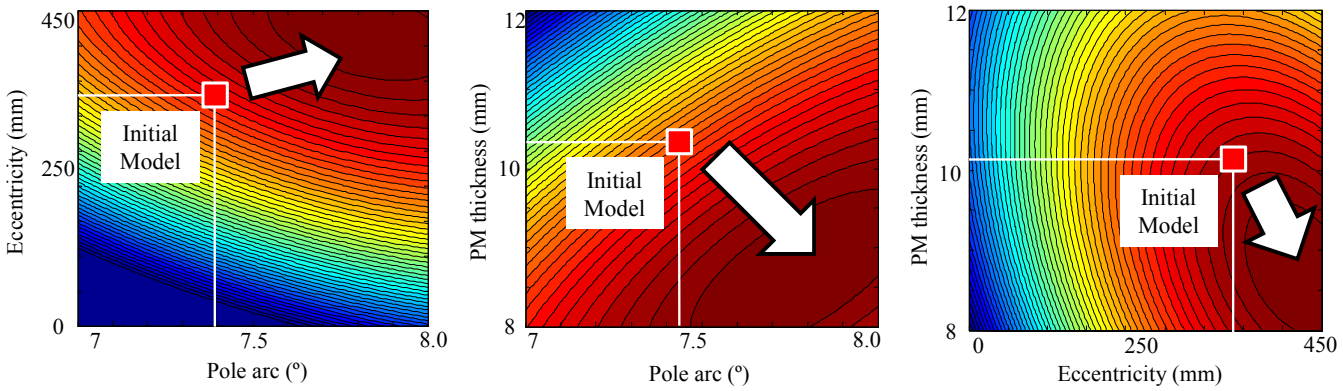

Fig. 8. Torque surface obtained through robust design optimization (RDO) according to design variables.

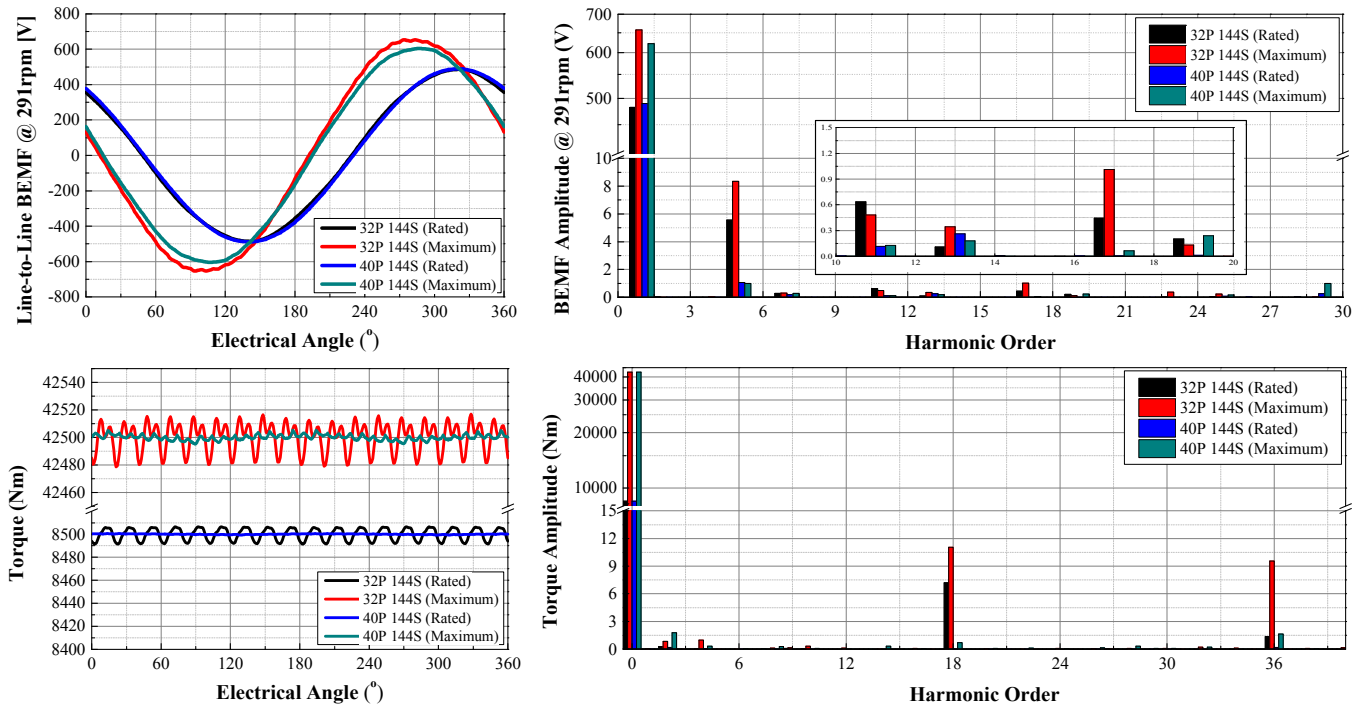

Fig. 10. Comparison of the line-to-line BEMF, the average torque waveforms, and their harmonics (prototype and designed optimum model).

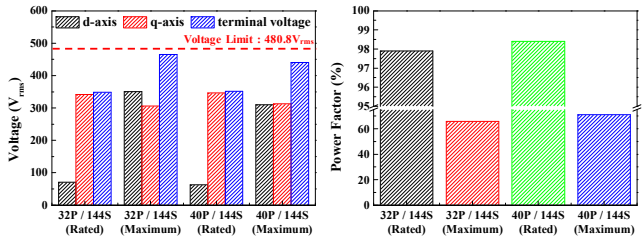

Fig. 11. Comparison of d-, q-, terminal voltages, and power factor (prototype and designed optimum model).

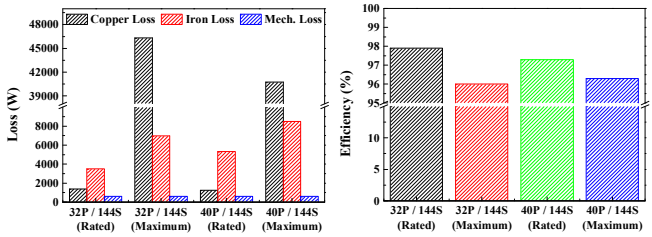

Fig. 12. Comparison of copper, iron, mechanical losses, and efficiency (prototype and designed optimum model).

TABLE III
COMPARISON OF PROTOTYPE AND DESIGNED OPTIMUM MODEL

Division	Prototype	Optimum Model	Unit
Type	Triple 3-Phase PMSM		-
Phase Shift	40	20	deg
Rated Torque	8500		Nm
Torque Ripple	0.18	0.01	%
Maximum Torque	42500		Nm
Torque Ripple	0.09	0.02	%
Power factor (Rated)	97.9	98.4	%
Efficiency (Rated)	97.9	97.3	%
Power factor (Maximum)	65.7	71.0	%
Efficiency (Maximum)	96.0	96.3	%

of torque ripple. The value was reduced from 0.01 to 0.004. Fig. 11 illustrates d-axis, q-axis, terminal voltages, and power factor. Two models achieves the voltage requirement and the designed model was superior than the prototype in terms of power factor. Fig. 12 shows copper, iron, mechanical losses, and efficiency. The rated efficiency of the designed model is decreased by 0.6% because of its increased pole number and iron loss. However, the maximum efficiency is increased by 0.3%. Finally, the effective radial force density and the deformation are shown in Fig. 13 and Fig. 14, respectively. Thanks to the increased vibration order of the radial magnetic force, the deformation of the designed model was decreased by half. Such validation proves that the designed model with 144-slot and 40-pole combination has the advantages in the electromagnetic and the vibratory characteristics than the prototype.

VII. CONCLUSION

This paper proposes a triple three-phase surface-mounted PMSM as a fascinating solution for ultra-high speed elevator direct drive applications and describes its multiphysics design procedure. Its specific verification and detailed design results was covered in this paper. It was proven that the designed optimum model with 144-slot and 40-pole combination exhibits the superior properties than the prototype.

VIII. REFERENCES

[1] S. I. Kim, S. Park, J. Cho, W. Kim, and S. Lim, "Investigation and experimental verification of a novel spoke-type ferrite magnet motor for electric-vehicle traction drive applications," *IEEE Trans. Ind. Electron.*, vol. *61,* no. *10,* pp. *5763-5770,* Oct. 2014.

[2] S. I. Kim, J. Cho, S. Park, T. Park, and S. Lim, "Characteristics comparison of a conventional and modified spoke-type ferrite magnet motor for traction drives of low-speed electric vehicles," *IEEE Trans. Ind. Appl.*, vol. *49,* no. *6,* pp. *2516-2523,* Nov./Dec. 2013.

[3] W. H. Kim, I. S. Jang, C. S. Jin, J. Lee, and S. G. Lee, "Design of novel overhang structure for separated pole-piece type ferrite magnet motor," *IEEE Trans. Magn.*, vol. 51, no. 3, pp. 1-4, Mar. 2015.

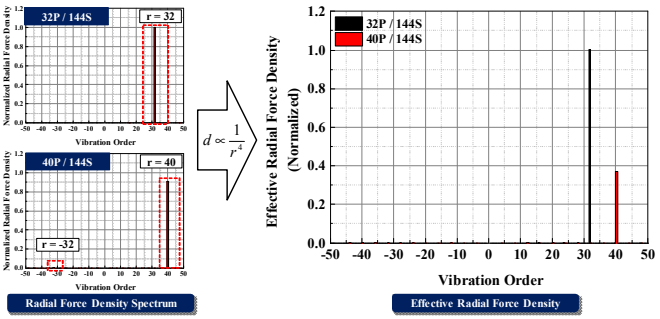

Fig. 13. Comparison of the effective radial force density considering the vibration order (prototype and designed optimum model).

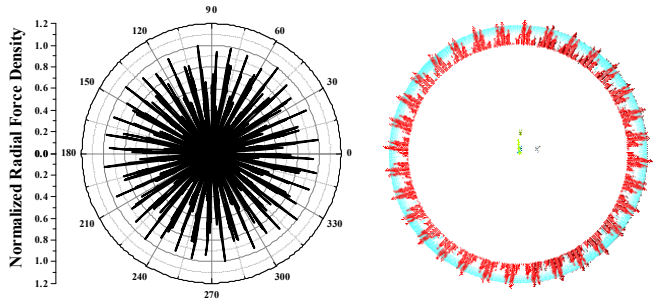

Fig. 14. Normalized radial force density and deformation distribution in polar axis (designed optimum model)

[4] I. Petrov and J. Pyrhonen, "Performance of low-cost permanent magnet material in PM synchronous machines," *IEEE Trans. Ind. Electron*., vol. 60, no. 6, pp. 2131-2138, Jun. 2013.

[5] Z. P. Xia, Z. Q. Zhu, L. J. Wu, and G. W. Jewell, "Comparison of radial vibration forces in 10-pole/12-slot fractional slot surface-mounted and interior PM brushless AC machines, in *Proc. IEEE ICEM*, Sep. 2010, pp. 1-6.

[6] W. Fei and P. C. K. Luk, "Investigation of radial electromagnetic force density and vibration in a fractional-slot interior permanent magnet synchronous machines, in *Proc. IEEE ECCE*, Sep. 2013, pp. 4998-5005.

[7] R. N. Lain and A. Bedford, "Recent developments in the design of gearless machines for elevators," in *Proc. IET Elec. Mach. Drives*, Sep. 1993, pp. 334-338.

[8] G. Wang, J. Qi, J. Xu, X. Zhang, and D. Xu, "Antirollback control for gearless elevator traction machines adopting offset-free model predictive control strategy," *IEEE Trans. Ind. Electron*., vol. 62, no. 10, pp. 6194- 6203, Oct. 2015.

[9] G. Wang, J. Xu, T. Li, G. Zhang, and H. Zhan, "Weight-transducerless starting torque compensation of gearless permanent-magnet traction machine for direct-drive elevators," *IEEE Trans. Ind. Electron*., vol. 61, no. 9, pp. 4594-4604, Sep. 2014.

[10] E. Jung, H. Yoo, S. K. Sul, H. S. Choi, and Y. Y. Choi, "A nine-phase permanent-magnet motor drive system for an ultrahigh-speed elevator," *IEEE Trans. Ind. Appl*., vol. 48, no. 3, pp. 987-995, May/Jun. 2012.

[11] H. S. Lim and R. Krishnan, "Ropeless elevator with linear switched reluctance motor drive actuation systems," *IEEE Trans. Ind. Electron*., vol. 54, no. 4, pp. 2209-2218, Aug. 2007.

[12] K. Yoshida and H. Matsumoto, "Propulsion and guidance simulation of a high-temperature superconducting bulk ropeless linear elevator," *IEEE Trans. Magn*., vol. 40, no. 2, pp. 615-618, Mar. 2004.

[13] S. G. Lee, S. A. Kim, S. Saha, Y. W. Zhu, and Y. H. Cho, "Optimal structure design for minimizing detent force of PMLSM for a ropeless elevator," *IEEE Trans. Magn*., vol. 50, no. 1, pp. 1-4, Jan. 2014.

[14] H. Fan, K. T. Chau, C. Liu, Z. Zhang, and C. Qiu, "Quantitive comparison of permanent magnet linear machines for ropeless elevator," in *Proc. IEEE IECON*, Nov. 2015, pp. 5357-5362.

[15] D. H. Kang, J. B. Ahn, J. W. Kim, and S. J. Jung, "Design of PM excited transverse flux linear motor with inner mover type," in *Proc. IEEE ICEMS*, Nov. 2003, pp. 242-245.

[16] Y. W. Zhu, S. G. Lee, and Y. H. Cho, "Optimal design of slotted iron core type permanent magnet linear synchronous motor for ropeless elevator system," in *Proc. IEEE ISIE*, Jul. 2010, pp. 1402-1407.

[17] M. S. Lim, S. H. Chai, J. S. Yang, and J. P. Hong, "Design and verification of 150-krpm PMSM based on experiment results of prototype," *IEEE Trans. Ind. Electron*., vol. 62, no. 12, pp. 7827-7836, Dec. 2015.

[18] L. Shao, W. Hua, Z. Q. Zhu, W. Huang, Z. Wu, F. Li, and M. Cheng, "Investigation on phase shift between multiple multiphase windings in flux-switching permanent magnet machines," *IEEE Trans. Ind. Appl.*, vol. 53, no. 3, pp. 1958-1970, May-Jun. 2017.

[19] F. Wu, P. Zheng, L. Cheng, and C. Zhou, "Analysis and experimental evaluation of harmonic leakage inductance for polyphase PM machines having close slot and pole combinations," *IEEE Trans. Magn*., vol. 51, no. 11, pp. 1-4, Nov. 2015.

[20] X. Liu and Z. Q. Zhu, "Winding configurations and performance investigations of 12-stator pole variable flux reluctance machines," in *Proc. IEEE ECCE*, Sep. 2013, pp. 1834-1841.

[21] D. Y. Kim, M. R. Park, J. H. Sim, and J. P. Hong, "Advanced method of selecting number of poles and slots for low-frequency vibration reduction of traction motor for elevator," *IEEE/ASME Trans. Mechatronics*, vol. 22, no. 4, pp. 1554-1562, Aug. 2017.

[22] G. Lei, J. Zhu, Y. Guo, C. Liu, and B. Ma, "A review of design optimization methods for electrical machines," *Energies*, vol. 10, no. 12, pp. 1-31, Nov. 2017.

[23] G. J. Park, T. H. Lee, W. H. Lee, and K. H. Hwang, "Robust design: an overview," *AIAA Journal*, vol. 44, no. 1, pp. 181-191, Jan. 2006.

IX. BIOGRAPHIES

Jae-Han Sim received the bachelor's degree in mechanical engineering and the master's degree in automotive engineering from Hanyang University, Seoul, South Korea, in 2012 and 2014, respectively, where he is currently working toward the Ph. D. degree in automotive engineering. His research focuses on a variety of electrical machines and their design optimization for automotive and industrial applications.

Dong-Gyun Ahn received the bachelor's degree in mechanical engineering and the master's degree in automotive engineering from Hanyang University, Seoul, South Korea, in 2012 and 2014, respectively, where he is currently working toward the Ph. D. degree in automotive engineering. His research focuses on various numerical techniques of the electromagnetic fields in the electrical machines.

Dae-Kee Kim received the bachelor's degree in mechanical engineering fr-om Hanyang University, Seoul, South Korea, in 2014, where he is currently working toward the Ph. D. degree in automotive engineering. His research interests include the electrical machine design for automotive applications, and the analytical approach of vibration and noise of electrical machines.

Dong-Kyun Son received the bachelor's degree in electrical engineering fr-om Ulsan University, Ulsan, South Korea, in 2017. He is currently working toward the Ph. D. degree in automotive engineering at Hanyang University. His research interests include the electrical machine design and the analytical approach of thermal analysis of electrical machines.

Saekyeol Kim received the bachelor's degree in mechanical engineering and the master's degree in automotive engineering from Hanyang University, Seoul, South Korea, in 2014 and 2016, respectively, where he is currently working toward the Ph. D. degree in automotive engineering. His research interests include design under uncertainty, robust design optimization and reliability-based design optimization.

Jung-Pyo Hong received the Ph. D. degree in electrical engineering from Hanyang University, Seoul, South Korea, in 1995. From 1996 to 2006, he was a Professor at Changwon National University, Changwon, South Korea. Since 2006, he has been a Professor with Hanyang University. His research interests include the electrical machine design, optimization, and numerical techniques.

Tae Hee Lee received the Ph. D. degree at the University of Iowa in 1991 and he is a Professor at the Department of Automotive Engineering, Hanyang University, Seoul, South Korea. His research interests include design optimization, design and analysis of computer experiments, design under uncertainty and surrogate model based optimization.